

**Alpacas in Space - An Autobiography**

By

JOSEPH LEVINE  
DISSERTATION

Submitted in partial satisfaction of the requirements for the degree of

DOCTOR OF PHILOSOPHY

in

Physics

in the

OFFICE OF GRADUATE STUDIES

of the

UNIVERSITY OF CALIFORNIA

DAVIS

Approved:

---

J. Anthony Tyson, Chair

---

S. Mani Tripathi

---

Brian Kolner

Committee in Charge

2025

# Abstract

An Afghan, an Albanian, an Algerian, an American, an Andorran, an Angolan, an Antiguans, an Argentine, an Armenian, an Australian, an Austrian, an Azerbaijani, a Bahamian, a Bahraini, a Bangladeshi, a Barbadian, a Barbudans, a Batswanan, a Belarusian, a Belgian, a Belizean, a Beninese, a Bhutanese, a Bolivian, a Bosnian, a Brazilian, a Brit, a Bruneian, a Bulgarian, a Burkinabe, a Burmese, a Burundian, a Cambodian, a Cameroonian, a Canadian, a Cape Verdean, a Central African, a Chadian, a Chilean, a Chinese, a Colombian, a Comoran, a Congolese, a Costa Rican, a Croatian, a Cuban, a Cypriot, a Czech, a Dane, a Djibouti, a Dominican, a Dutchman, an East Timorese, an Ecuadorean, an Egyptian, an Emirian, an Equatorial Guinean, an Eritrean, an Estonian, an Ethiopian, a Fijian, a Filipino, a Finn, a Frenchman, a Gabonese, a Gambian, a Georgian, a German, a Ghanaian, a Greek, a Grenadian, a Guatemalan, a Guinea-Bissauan, a Guinean, a Guyanese, a Haitian, a Herzegovinian, a Honduran, a Hungarian, an I-Kiribati, an Icelander, an Indian, an Indonesian, an Iranian, an Iraqi, an Irishman, an Israeli, an Italian, an Ivorian, a Jamaican, a Japanese, a Jordanian, a Kazakhstani, a Kenyan, a Kittian and Nevisian, a Kuwaiti, a Kyrgyz, a Laotian, a Latvian, a Lebanese, a Liberian, a Libyan, a Liechtensteiner, a Lithuanian, a Luxembourger, a Macedonian, a Malagasy, a Malawian, a Malaysian, a Maldivan, a Malian, a Maltese, a Marshallese, a Mauritanian, a Mauritian, a Mexican, a Micronesian, a Moldovan, a Monacan, a Mongolian, a Moroccan, a Mosotho, a Motswana, a Mozambican, a Namibian, a Nauruan, a Nepalese, a New Zealander, a Nicaraguan, a Nigerian, a Nigerien,

a North Korean, a Northern Irishman, a Norwegian, an Omani, a Pakistani, a Palauan, a Palestinian, a Panamanian, a Papua New Guinean, a Paraguayan, a Peruvian, a Pole, a Portuguese, a Qatari, a Romanian, a Russian, a Rwandan, a Saint Lucian, a Salvadoran, a Samoan, a San Marinese, a Sao Tomean, a Saudi, a Scottish, a Senegalese, a Serbian, a Seychellois, a Sierra Leonean, a Singaporean, a Slovakian, a Slovenian, a Solomon Islander, a Somali, a South African, a South Korean, a Spaniard, a Sri Lankan, a Sudanese, a Surinamer, a Swazi, a Swede, a Swiss, a Syrian, a Tajik, a Tanzanian, a Togolese, a Tongan, a Trinidadian or Tobagonian, a Tunisian, a Turk, a Tuvaluan, a Ugandan, a Ukrainian, a Uruguayan, a Uzbekistani, a Venezuelan, a Vietnamese, a Welshman, a Yemenite, a Zambian and a Zimbabwean

all go to a bar..

The doorman stops them and says "Sorry, I can't let you in without a Thai."

# Contents

<b>Contents</b>	<b>iv</b>
<b>List of Figures</b>	<b>v</b>
<b>List of Tables</b>	<b>vi</b>
<b>1 The Dark Matter Story</b>	<b>3</b>
<b>2 Experiment Overview and Design</b>	<b>7</b>
2.1 Sources of Power in Measured Spectrum . . . . .	9
2.2 Toy Analysis . . . . .	18
2.3 Thermal Noise in A Cavity . . . . .	18
2.4 Reverberation Chambers and Statistical Uniformity . . . . .	18
2.5 System Design . . . . .	18
<b>3 System Characterization and Data Acquisition</b>	<b>36</b>
3.1 Control and Quantifying of Uncertainties . . . . .	38
<b>4 Data Analysis and Calibration</b>	<b>39</b>
<b>5 Beyond 300 MHz</b>	<b>41</b>
<b>Bibliography</b>	<b>42</b>

# List of Figures

1.1	Expected vs observed velocity distributions of M33 . . . . .	4
1.2	Dark matter mass regimes . . . . .	6
2.1	An antenna and matched resistor in cavities which are in thermal equilibrium.	13
2.2	Schematic of LNA adding input referred noise . . . . .	16
2.3	Schematic of the RF receiver system . . . . .	19
2.4	Spectrum from veto antenna during 300MHz data run . . . . .	22
2.5	Photo of set up to measure Shielding effectiveness of shielded room . . . . .	23
2.6	Shielding effectiveness of shielded room, 50-300 MHz . . . . .	24
2.7	Shielding effectiveness of shielded room, 125-3000 MHz . . . . .	25
2.8	AB-900A biconical antenna free space effective aperture, simulated, measured and theoretical . . . . .	27
2.9	simulated AB-900A biconical antenna free space complex input impedance, vs measured biconical data . . . . .	28
2.11	Schematic of Interlock board . . . . .	30
2.12	Photo of lead-acid battery and slow turn on circuit . . . . .	31
2.13	Acquisition efficiency for GPU-based Real-time spectrum analyzer . . . . .	33
3.1	Data stream of real time DAQ. This set up is duplicated for channels A and B .	38
3.2	Gain vs. voltage of front end amplifier . . . . .	38

# List of Tables

2.1 Specifications for the spectrum analyzer used for run 1A. . . . .	32
-----------------------------------------------------------------------	----

## **Acknowledgments**

Thank you to: Ben Dave Hemmer Monda Bill Tuck Buchholtz/Ayars/Nelson/Kagan/Clare/Patrova/Rick Danner/pechkis  
Belva Mr keye Bill Nye

Self plagiarism statement <https://journals.aps.org/copyrightFAQ.html>

As the author of an APS-published article, may I include my article or a portion of my article in my thesis or dissertation? Yes, the author has the right to use the article or a portion of the article in a thesis or dissertation without requesting permission from APS, provided the bibliographic citation and the APS copyright credit line are given on the appropriate pages.

<https://grad.ucdavis.edu/preparing-filing-your-thesis-or-dissertation>

Published or publishing pending material may be used with permission from the copyright owner, if not you, and the Graduate Chair, if you are not the first-author. See the Copyright FAQ for information about permissions when using published material.

Material you have authored, and which has been previously published or is pending publishing, may be used in its published format with three exceptions: 1) Margins - You must maintain 1" margins on all sides throughout the paper. 2) Pagination - page numbers must follow the UC Davis standards. 3) The title page must follow UC Davis standards and you must include an overall abstract.

File: thesis.tex

Encoding: utf8

Sum count: 2406

Words in text: 2185

Words in headers: 51

Words outside text (captions, etc.): 94

Number of headers: 13

Number of floats/tables/figures: 4

Number of math inlines: 69

Number of math displayed: 7

Subcounts:

text+headers+captions (#headers/#floats/#inlines/#displayed)

644+6+0 (2/0/0/0) \_top\_

369+4+71 (1/2/3/0) Chapter: The Dark Matter Story

310+4+0 (1/0/0/0) Chapter: Experiment Overview and Design

29+6+0 (1/0/0/1) Section: Sources of Power in Measured Spectrum

234+8+0 (3/0/34/6) Subsection: Thermal Noise

12+0+0 (0/0/8/0) Subsection: Dark Photon Signal

6+0+0 (0/0/3/0) Subsection: Radio Frequency Interference

19+0+0 (0/0/10/0) Subsection: LNA Noise

9+0+0 (0/0/5/0) Subsection: Shielded room

2+0+0 (0/0/2/0) Subsection: Antenna

0+0+0 (0/0/0/0) Subsection: Spectrum Analyzer Details

309+5+16 (1/1/3/0) Chapter: System Characterization and Data Acquisition

0+5+0 (1/0/0/0) Section: Control and Quantifying of Uncertainties

3+6+7 (1/1/0/0) Subsection: Direct Measurement of Amp Chain Parameters

233+4+0 (1/0/1/0) Chapter: Data Analysis and Calibration

6+3+0 (1/0/0/0) Chapter: Beyond 300 MHz

(errors:2)

# Chapter 1

## The Dark Matter Story

If we start making a list of things that aren't here, we could be here all night. You know, pens for instance. Let's stick with things we can see.

---

Wheatley

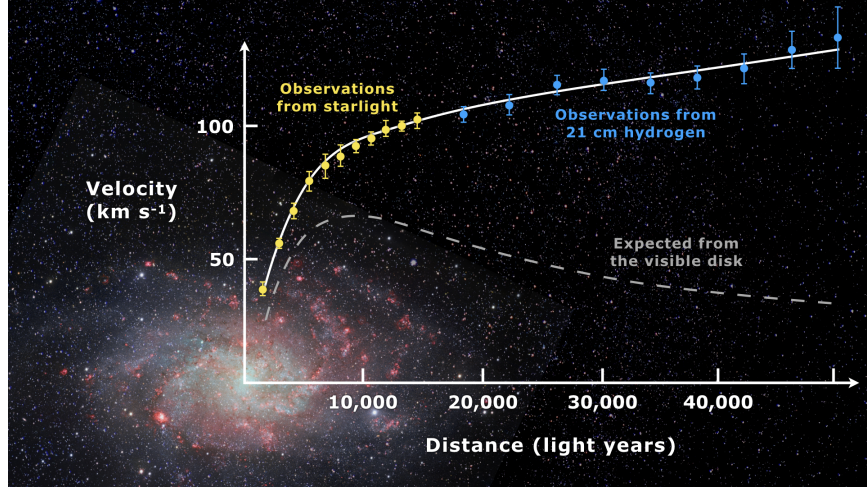


Figure 1.1: Expected vs observed velocity distributions of M33

It is believed that a large majority of the mass in the universe comes from an as yet undetermined source. This claim stems originally from work performed in 1933 by Fritz Zwicky who noticed a discrepancy between measured velocities of galaxies within the Coma Cluster and velocities predicted by applying the virial theorem. He wrote

*If this [experimental result] would be confirmed we would get the surprising result that dark matter is present in much greater amount than luminous matter [1].*

Vera Rubin furthered this work by measuring velocities of stars rotating in the M31 galaxy and concluded there must be additional non-luminous mass (originally published in [2], and shown in Fig.1.1). Studies of other phenomena, such as lensing (see [**lensing2**]) have confirmed the existence of this dark matter, and it is currently one of the major mysteries in modern physics.

Since the 1980's, the leading theories have consisted of an unknown species of elementary

particle. The search for weakly interacting massive particles (WIMPs) have dominated the budgets and schedules of the dark matter search effort but have yet to provide any experimental evidence.

In light of this, the 2017 community report on dark matter [3] highlights a need for a multi-experiment program in which many small scale experiments ( $< \$10M$ ) split up to cover the vast landscape of potential dark matter candidates (see Fig. 1.2). Since very little is known about the dark matter, it is a playground for theoretical physicists to invent candidates. This overwhelming search should be narrowed down.

The enormous mass range splits nicely into two regimes; waves and particles. At a mass of order 1eV the inter-particle spacing  $\approx$  wavelength. Lighter than this it is more convenient to think of dark matter as a wave. Alternatively, dark matter candidates heavier than this are more conveniently modeled as exhibiting particle-like behavior. The Dark E-Field Radio experiment searches for dark photons in the nano- to milli-eV mass range where dark matter is best described as a wave. This property means one would search for a dark photon using wave-like detectors, e.g. antennas.

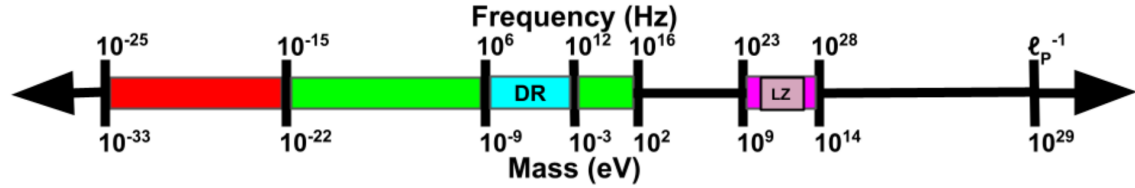


Figure 1.2: Cartoon depicting the mass scales over which dark matter may be found. Corresponding frequencies shown above. At heavy mass scales  $> \mathcal{O}(1\text{ eV})$  the dark matter would behave like a particle, while on the lighter end it would behave like a wave. The Dark Radio Experiment searches at radio/microwave frequencies (blue) for a hidden photon using an antenna and spectrum analyzer. LUX-ZEPLIN Experiment (LZ) also shown.

# Chapter 2

## Experiment Overview and Design

A month in the laboratory can  
often save an hour in the  
library.

---

Frank Westheimer

Veljko Radeka said of detectors “One would imagine that in each particular case the best solution is arrived at by 1) the detector design to maximize the significant signal, 2) reduction of noise at its physical source, and 3) optimum filtering of signal and noise.” [4]. While he was referring to position sensitive particle detectors, the same three principles apply to this experiment. Put more directly, the goal is to maximize the signal to noise ratio. The detector in this case is a low-noise, wide-band radio receiver system searching not for discrete instances of particle-like interactions, but for coherent waves which are constant over long periods. The signal is a small excess of narrow-band, radio frequency power received by an antenna in a cavity. The noise is the white, thermal background due to the 300 K walls. The system is shown schematically in Fig. 2.3.

This chapter begins with a section titled Toy Analysis which walks through several back-of-the-envelope calculations to follow the signal and noise as it progresses from fields in free space through a simplified detector, resulting in a (simulated) dark photon detection. Through this section, several important concepts will come up and their implications can be analyzed. This will result in intuition which will explain the remaining design choices of Sec. 2.5. Furthermore, the actual experiment will report a null result, i.e. a lack of detection of a signal on a background. By following a signal *forward* through the system and data analysis, it will be more clear how to infer an exclusion limit from a power spectrum and working *backward* through the experiment.

In the following two sections, 2.3 and 2.4, effects will be introduced that were not apparent from the simplistic analysis of the first section. The final section, 2.5, details each piece of the system.

## 2.1 Sources of Power in Measured Spectrum

This section will break down each term in the following equation for the input-referred power

$$P_i = \text{Thermal Noise} + \text{Dark Photon Signal} + \text{RFI} + \text{LNA Noise} + \text{ADC Noise}/G. \quad (2.1)$$

Where G is a gain factor, and each term will be addressed in subsections 2.1.1 - 2.1.5.

### 2.1.1 Thermal Noise

#### 2.1.1.1 Blackbody Electric Field Density

This sub section estimates the noise-like electric field in free space due to black body radiation. It assumes to be in *some* enclosure in that the ambient temperature is known to be 300 K and not the 3.6 K of the sky.

Planck's law gives the black body spectral energy density as

$$u_\nu(\nu, T) d\nu = \frac{8\pi h\nu^3}{c^3} \frac{1}{e^{h\nu/kT} - 1} d\nu \quad \left[ \frac{J}{m^3} \right]. \quad (2.2)$$

This is frequently written in terms of spectral radiance,

$$B_\nu(\nu, T) d\nu = \frac{2h\nu^3}{c^2} \frac{1}{e^{h\nu/kT} - 1} d\nu d\Omega \quad \left[ \frac{W}{m^2} \right]. \quad (2.3)$$

Integrating this isotropic radiance over a solid angle  $4\pi$  sr as well as a small frequency band  $\Delta\nu$  gives the flux density  $|\mathbf{S}|$  (AKA, the magnitude of the Poynting vector),

$$\begin{aligned}
|\mathbf{S}| &= \int_0^{4\pi} \int_{\nu}^{\nu+\Delta\nu} B_{\nu}(\nu, T) d\nu d\Omega \\
&= \int_0^{4\pi} \int_{\nu}^{\nu+\Delta\nu} \frac{2h\nu^3}{c^2} \frac{1}{e^{h\nu/kT} - 1} d\nu d\Omega \quad \left[ \frac{W}{m^2} \right] . \\
&\approx \frac{8\pi h\nu^3}{c^2} \frac{1}{e^{h\nu/kT} - 1} \Delta\nu
\end{aligned} \tag{2.4}$$

The flux density can be related to the rms electric field from Poynting's theorem

$$|\mathbf{S}| = \frac{|E_{\text{rms}}|^2}{\eta} \quad \left[ \frac{W}{m^2} \right], \tag{2.5}$$

where  $\eta$  is the impedance of free space. Equating Eqs. 2.4 and 2.5 and solving for the electric field gives

$$\frac{|E_{\text{rms}}|}{\sqrt{\Delta\nu}} = \sqrt{\eta \frac{8\pi h\nu^3}{c^2} \frac{1}{e^{h\nu/kT} - 1}} \quad \left[ \frac{V}{m \cdot \sqrt{\text{Hz}}} \right]. \tag{2.6}$$

This equation breaks up nicely into two regimes

$$\frac{|E_{\text{rms}}|}{\sqrt{\Delta\nu}} = \begin{cases} \sqrt{\eta \frac{8\pi kT\nu^2}{c^2}} & \text{Rayleigh-Jeans regime } (h\nu \ll kT) \\ \sqrt{\eta \frac{8\pi h\nu^3}{c^2} e^{-h\nu/kT}} & \text{Wien approximation } (h\nu \gg kT) \end{cases} \quad \left[ \frac{V}{m \cdot \sqrt{\text{Hz}}} \right]. \tag{2.7}$$

At frequencies and temperatures where the experiment is operated ( $< 300 \text{ MHz}$  and  $300 \text{ K}$ ),  $h\nu/kT \lesssim 5 \times 10^{-5}$  suggesting the Rayleigh-Jeans approximation is valid. At  $300 \text{ K}$ , this yields electric field spectral densities of  $1$  and  $6 \text{ nV/m}\sqrt{\text{Hz}}$  at  $50$  and  $300 \text{ MHz}$  respectively.

It is interesting to note, however, that for cryogenic experiments operating at a few GHz and in the sub K range,  $h\nu/kT \approx 1$  and the full form of Eq. 2.6 must be used.

### 2.1.1.2 Antenna Noise

An antenna's effective aperture,  $A_e$  [m<sup>2</sup>], represents the effective area that it has to collect power density or irradiance [W/m<sup>2</sup>] from an incident Poynting vector,

$$P_A = |\mathbf{S}|A_e, \quad (2.8)$$

Where  $|\mathbf{S}|$  is the magnitude of the incident Poynting vector and  $P_r$  is the power received at the antenna which is available at its terminals.

$A_e$  is a directional quantity which varies with the antenna's directivity  $D(\Omega)$ , where  $\Omega$  represents solid angle around the antenna. It varies with frequency  $\nu$ , though it is generally discussed in terms of wavelength  $\lambda$ . Three matching parameters are introduced to describe how much actual power the antenna is able to deliver to a transmission line;  $p$  the polarization match of the wave to the antenna,  $m$  the impedance match of the antenna to the transmission line and  $\eta_a$  the efficiency of the antenna which represents how much power is absorbed compared to that lost to Joule heating of the antenna.  $p$ ,  $m$  and  $\eta_a$  are all real, dimensionless and vary between 0 and 1.

$$A_e \equiv \frac{\lambda^2}{4\pi} D(\Omega) p m \eta_a. \quad (2.9)$$

This definition follows [5], though some authors do not include  $p$  in the definition [6] [7].

A simple derivation of the direction-averaged effective aperture based on thermodynamics will provide intuition. An isotropic antenna placed in a cavity at temperature T will be illuminated by randomly polarized, isotropic radiation of the form given by the Rayleigh-

Jeans limit of Eq. 2.4,  $|\mathbf{S}| = 8\pi kT\Delta\nu\nu^2/c^2$ . The power received by the antenna can be found by Eq. 2.8,

$$\begin{aligned} P_A &= \langle A_e \rangle \frac{1}{2} |\mathbf{S}| \\ &= \langle A_e \rangle \frac{4\pi kT\nu^2}{c^2} \Delta\nu, \end{aligned} \quad (2.10)$$

Where the factor of  $1/2$  is introduced to account for the random polarization and the  $\langle \cdot \rangle$  indicate an average aperture over all angles around the antenna. If a resistor is placed in a second cavity, also at temperature  $T$ , by it will deliver

$$P_R = kT\Delta\nu \quad (2.11)$$

into a matched transmission line. This is shown in Fig. 2.1. The second law of thermodynamics makes a very powerful statement here; the net power flow must equal 0 if the two temperatures are indeed equivalent. This means  $P_R = P_A$  or Eq. 2.10 = Eq. 2.12,

$$\begin{aligned} \langle A_e \rangle \frac{4\pi kT\nu^2}{c^2} \Delta\nu &= kT\Delta\nu \\ \langle A_e \rangle &= \frac{c^2}{4\pi\nu^2} \quad [\text{m}^2] \\ &= \frac{\lambda^2}{4\pi} \end{aligned} \quad (2.12)$$

This allows us to conclude that the power spectral density  $S_{\text{ant}}$  received by an antenna surrounded by an isotropic temperature is simply  $kT\Delta\nu$  in the Rayleigh-Jeans limit of room temperatures and standard electronic frequencies. This gives a power which is equivalent to the well known result for a resistor at 290 K,

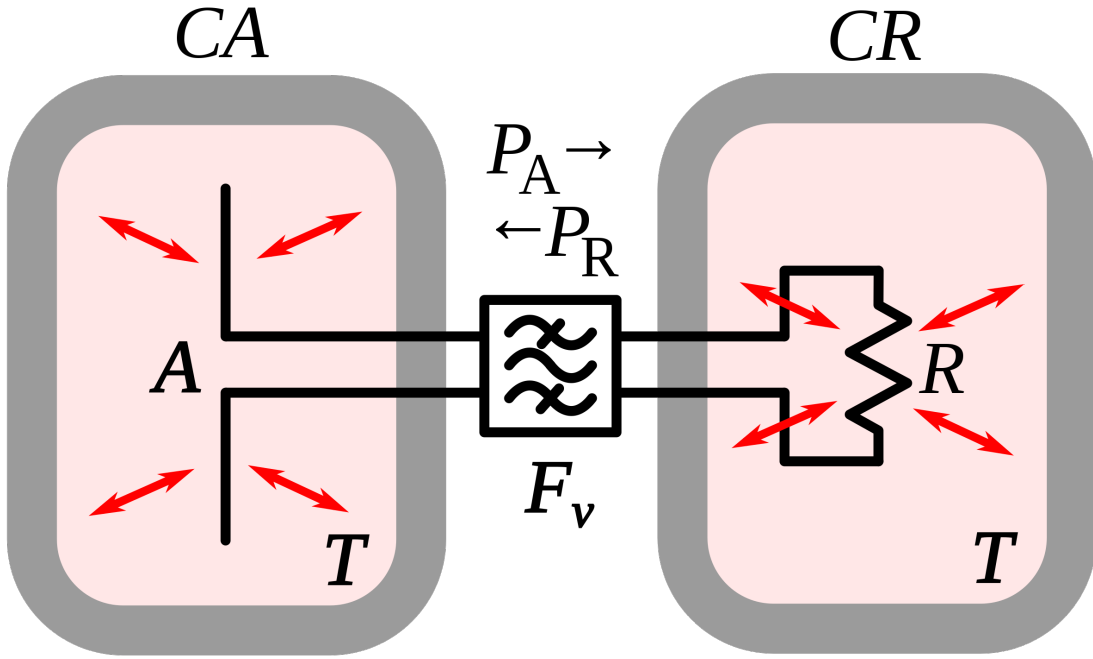


Figure 2.1: An antenna and matched resistor in cavities which are in thermal equilibrium. They are connected by a narrow filter permitting a narrow frequency band  $\Delta\nu$ . Image from Wikipedia.

$$S_{\text{ant}} = 3.9 \times 10^{-22} [\text{W}/\text{Hz}] = -174 [\text{dBm}/\text{Hz}]. \quad (2.13)$$

Note that  $S_{\text{ant}}$  indicates power spectral density and should not be confused with  $\mathbf{S}$  which indicates a Poynting vector.

#### 2.1.1.3 Noise as a Statistical Process

Equation 2.13 gave the mean of a power spectrum which is inherently noisy. This spectrum can be modeled with the Dicke radiometer equation. The measured power (assuming only thermal noise) is given by

$$P_{\text{ant}} = kT\Delta\nu \left(1 \pm \frac{1}{\sqrt{\Delta\nu\tau}}\right) \quad [\text{W}]. \quad (2.14)$$

Here  $\tau$  is the total acquisition time and so  $\Delta\nu\tau$  is equivalent to the number of spectra that are averaged together.

Thus far the analysis has focused only on thermal noise, however there are other sources of noise and interfering signals which must be considered, not to mention the actual signal dark photon signal.

### 2.1.2 Dark Photon Signal

The electric field of a kinetically mixed dark photon in free space  $\mathbf{E}_{\text{ant}}^{\text{free space}}$  was derived in Sec. XXX. In a cavity, the E-field will be enhanced by the quality factor  $Q$  of the cavity. This  $Q$  must be measured or simulated, but for this toy analysis we will assume it to be known<sup>1</sup>. The E-field inside the cavity then is

$$\mathbf{E}_{\text{ant}} = \mathbf{E}_{\text{ant}}^{\text{free space}} \sqrt{Q}, \quad (2.15)$$

since  $Q$  is proportional to power, i.e.  $\mathbf{E}^2$ . This E-field will then need to be converted from a wave in the cavity to a wave in a  $50\Omega$  transmission line by an antenna. Similar to the thermal noise of the previous section, this electric field will be converted via the effective aperture of the antenna. Similar to  $Q$ , aperture will be assumed to be known.

The total received power from a coherent signal inside the room then is

$$P = \frac{\mathbf{E}_{\text{ant}}^{\text{free space}^2}}{\eta} Q < A_e >, \quad (2.16)$$

---

<sup>1</sup>Typical values are in the ballpark of 100. Some experiments have ultra-high  $Q$  cavities  $\approx 10^{10}$  [8]

where  $\eta$  is the impedance of free space.

### 2.1.3 Radio Frequency Interference

Radio Frequency Interference (RFI) includes any coherent interfering signals which can be detected by the experiment. While noise is better described as a power spectral density [W/Hz] or electric field density [V/(m Hz)], RFI is made up of more narrow lines and is discussed in terms of a power [W] or electric field [V/m]. In this experiment, RFI is mitigated through the shielding effectiveness (SE) of the cavity. SE measurements and more details about local RFI are discussed further in Sec. 2.5.1, and a plot of the local RFI spectrum is shown in Fig. 2.4.

The peak RFI spike is at 186 MHz and approximately  $100 \mu\text{V}/\text{m}$ , an energy density of roughly  $10^{-11} \text{ W}/\text{m}^2$ . This will be reduced by the SE of the room (roughly 120 dB at 200MHz, see Fig. 2.5), but just like a coherent dark photon, it will be enhanced by the Q/effective aperture. This will be right on the edge of detection, but in the actual date run it was not detected.

### 2.1.4 LNA Noise

Any amplifier will have some noise which it adds to an incoming signal which will degrade the signal to noise ratio (SNR) of the measurement. A low noise amplifier (LNA) is an amplifier which has been specifically designed to minimize the noise contribution. This process is shown schematically in Fig. 2.2.

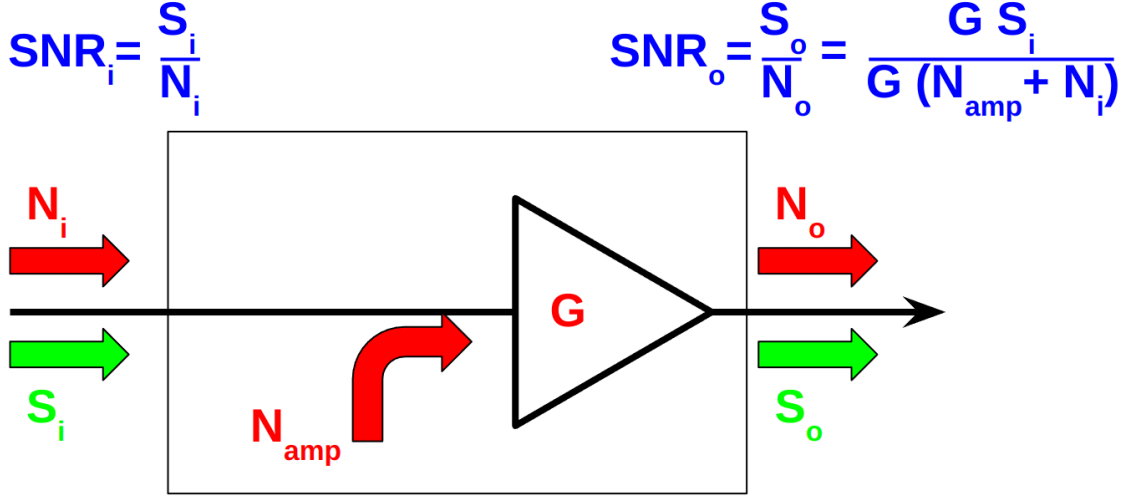


Figure 2.2: Schematic of LNA adding input referred noise  $N_{\text{amp}}$ . Since  $N_{\text{amp}}$  is referred to the input, it can be directly added to the input noise which is itself input-referred. The amplifier (depicted as a triangle) is assumed to be noiseless, while the physical amplifier including noise is contained in the rectangle.

The performance of an LNA is generally evaluated by a figures of merit and noise factor (F). F is defined to be the ratio the SNR at the input of an LNA to that at its output.

$$\begin{aligned}
 F &\equiv \frac{\text{SNR}_i}{\text{SNR}_o} \\
 &= \frac{S/N}{[S G]/[(N + N_{\text{amp}})G]} \\
 &= \frac{1}{1/[1 + N_{\text{amp}}/N]} \\
 &= 1 + \frac{N_{\text{amp}}}{N},
 \end{aligned} \tag{2.17}$$

where  $S$  and  $N$  are the signal and noise [W] presented to the LNA respectively,  $N_{\text{amp}}$  is the input-referred noise added by the LNA and  $G$  is the gain. By factoring out the implicit  $k \Delta\nu$  from  $N = kT\Delta\nu$ , we find

$$F = 1 + \frac{T_e}{T_0}, \quad (2.18)$$

where  $T_e$  is the noise temperature of a device and  $T_0$  the temperature of the system being measured by the LNA. In order to standardize device specifications for unknown system applications, it is common to choose a reference temperature  $T_0$  of 290K. If not specified, it is generally safe to assume this has been done.

Noise factor is simply defined from noise figure,

$$\text{NF} \equiv 10\log_{10}(F). \quad (2.19)$$

When working with LNAs, all three measurements ( $T_e$ ,  $F$  and NF) are frequently used and one must use Eqs. 2.18 and 2.19 to convert between them.

Noise figures are typically frequency dependant, though vary slowly over frequency and can be approximated as constant over narrow frequency bands. Noise figures are typically given on the data sheet of the LNA [9], but can also be measured. Measurement of LNA noise is covered in Sec. XXX and is shown in Fig. XXX.

The power contributed by the LNA's noise is simply given by

$$P_{\text{LNA}} = kT_e\Delta\nu \quad (2.20)$$

This is again the mean of a fluctuating power, just as 2.14.

### **2.1.5 ADC Noise**

ADC noise refers to the noise introduced by an Analog-to-Digital Converter during the process of converting an analog signal into a digital signal.

## **2.2 Toy Analysis**

### **2.3 Thermal Noise in A Cavity**

### **2.4 Reverberation Chambers and Statistical Uniformity**

Generally it is convenient to think of electromagnetic cavities as containing a single mode

## **2.5 System Design**

This section outlines the subsystems which make up the experiment. While specifics and basic calculations are provided as they apply to design choices of subsystems, testing and characterisation of the system as a whole is covered in Ch. 3 and calibration of the system is discussed in Ch. 4.

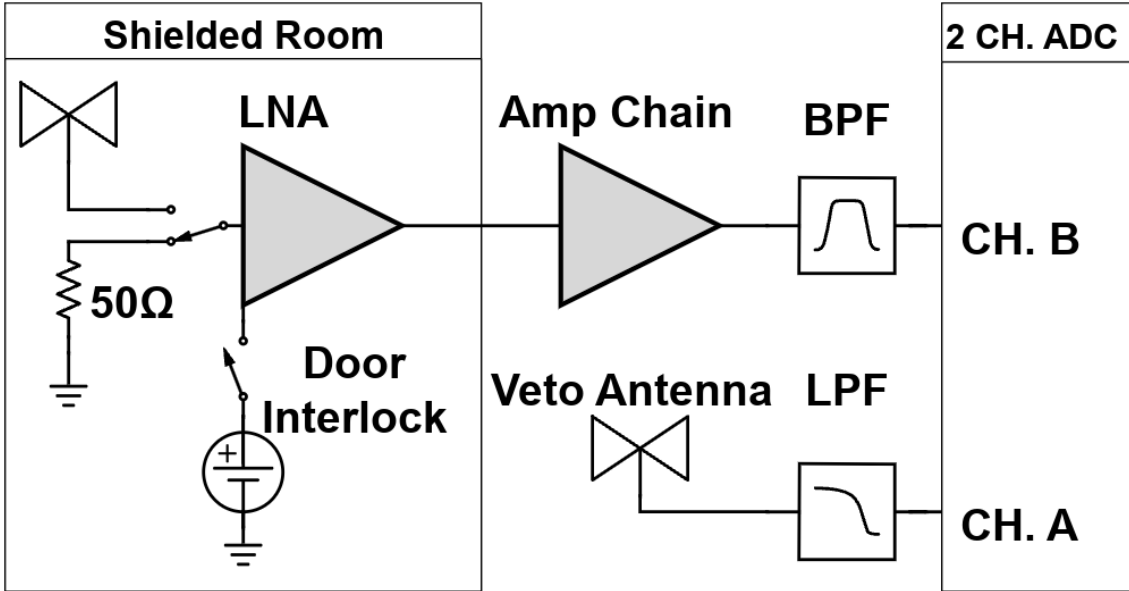


Figure 2.3: Schematic of the RF receiver system. An RF coax switch allows the PC to control the source (antenna or terminator). The switch is controlled by optical fiber to maintain isolation of the room. The LNA (Pasternack PE15A1012) has a nominal gain and noise temperature of 40dB and 100K (Figs. XXX and XXX). It is interlocked (Fig. 2.11) to the door to protect amp B and the ADC from large signals when the door is open. The secondary amplifier is a miniCircuits (MC) ZKL-1R5+ and has a nominal gain of 38dB. Not pictured after this amplifier is a fixed 4dB of attenuation. The band pass filter (BPF) is made up of a MC SLP-50+ high pass filter (HPF) and a MC ZX75LP-288-S+ low pass filter. The HPF reduces the bandwidth and therefore the total power of the signal before entering the ADC allowing for more gain before clipping. The LPF serves the same purpose while also acting as an anti-aliasing filter. These two filters define the experiment's bandwidth,  $-3 \text{ dB} \approx 40 - 320 \text{ MHz}$ . The veto antenna is outside of the room and interference is not reduced by the  $\approx 100 \text{ dB}$  SE of the room, so no gain is required. The LPF on the veto is for anti-aliasing.

### 2.5.1 Shielded room

The shielding room [10] serves two purposes. The first is straightforward; to shield the antenna, keeping radio frequency interference (RFI) *out*. The second purpose is a bit more subtle; to keep any converted dark photons *in*. This second point is addressed further as an

aspect of system calibration in Ch. 4, but roughly can be described by the loaded quality factor [11–13] of the antenna/room system. Namely, a more resonant system will be more sensitive to coherent signals. This subsection will focus on the first point, keeping RFI out.

Shielding effectiveness SE is a measurement of a shielding enclosure’s ability to attenuate electromagnetic waves from entering,

$$SE \equiv 10 \log_{10} \left( \frac{P_{\text{open}}}{P_{\text{closed}}} \right) = P_{\text{open}, dB} - P_{\text{closed}, dB} \quad (2.21)$$

where  $P_{\text{open}}/P_{\text{closed}}$  are powers received with the door open/closed. The ratio of powers allows all the specifics of antenna matching to cancel allowing for a very simple measurement.

Due to reciprocity between antennas, this is equivalent to measuring the attenuation of waves leaving. The latter method is simpler and was performed. The IEEE standard prescribing a very detailed SE measurement procedure [14] was used as a rough guideline but the simple results presented here should be viewed as an estimate.

The SE was measured by placing a Rigol DSG-830 signal generator inside the room, powered by the filtered 12 VAC Edison outlets inside the room. An antenna (bicon or Vivaldi) was connected to the signal generator. Outside of the room, an identical antenna (again, bicon or Vivaldi) was connected to a Rigol RSA-5065-TG spectrum analyzer. The spectrum is scanned to find a frequency without local interference which would confuse the results. The spectrum analyzer was set to attenuate its input to prevent clipping<sup>2</sup>, and the signal generator was set to output a sine wave at maximum power. The power measured on

---

<sup>2</sup>The spectrum analyzer automatically calibrates the displayed spectrum to its internal attenuator and pre-amplifier. If external gain/attenuation are used, they must be accounted for manually.

the spectrum analyzer is  $P_{\text{open}}$  of Eq. 2.21. The door was closed, attenuation removed and  $P_{\text{closed}}$  was measured. In some cases the SE was so high a signal was buried below the noise floor of the spectrum analyzer. These data are shown in red in Figs. 2.6 2.7.

SE can drop off to less than 80dB if the RF gasket around the door is not clean. Previous day-long test runs detected several hundred signals which originated from RFI emitted from the PC and several local radio stations. Cleaning was performed by scrubbing the copper gasket and steel mating surface with red scotch-brite using denatured alcohol as a lubricant. After two passes of polishing were complete, a layer of Deoxit D100L liquid was added. Maintenance cleanings were performed using only Deoxit D5 spray. These signals were not detected after the gasket was cleaned, which is consistent with calculations of Sec. XXX

The primary RFI in the 50-300 MHz span are from local radio broadcasts. The strongest of this is around  $100 \mu\text{V}/\text{m}$  as measured in the lab. There are also many lower level peaks which span the entire frequency range, though are more pronounced in a few frequency bands (60-75MHz, 130-140Mhz, 270-290MHz). These peaks come from the PC which serves as the spectrum analyzer. Before the door was cleaned, many of these signals were detectable, but cleaning the door resulted in a clean spectrum for the 9 day data run. The spectrum from the veto antenna (discussed in Sec. XXX) is shown in Fig. 2.4

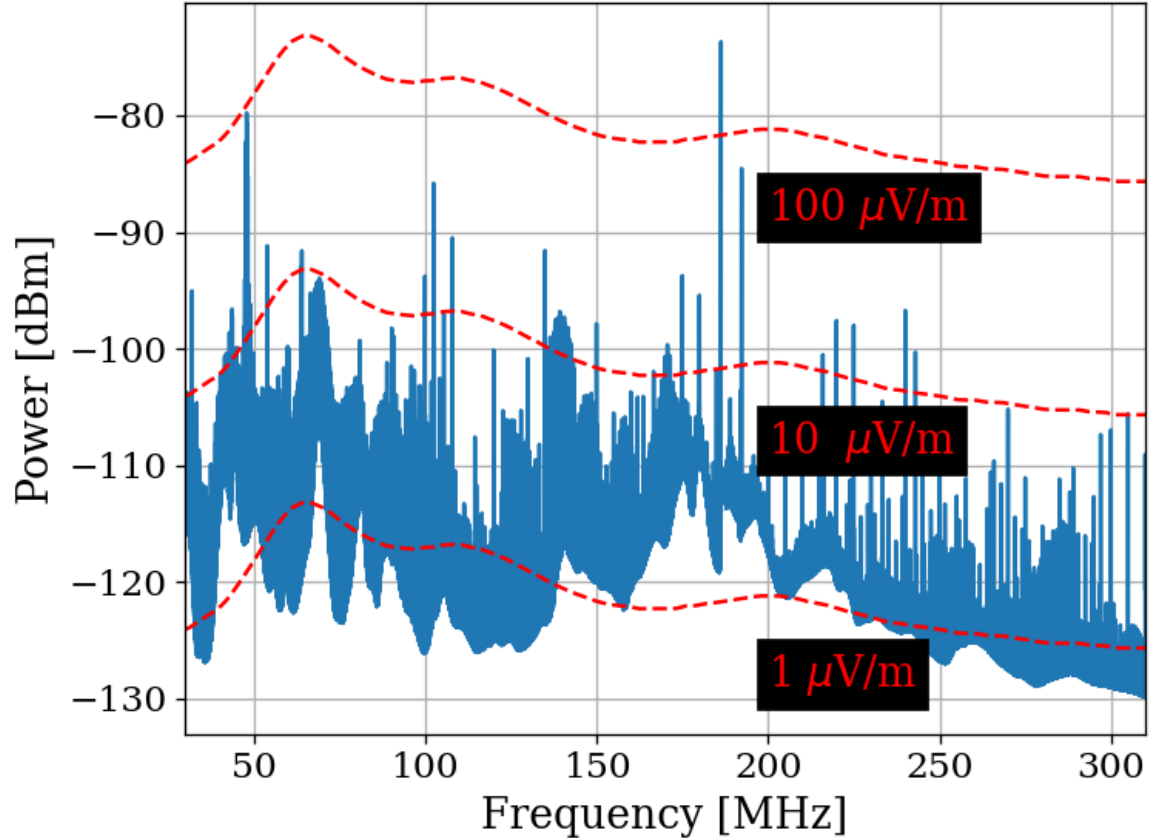


Figure 2.4: Spectrum from veto antenna during 300MHz data run. Spectrum plotted as measured power in dBm. Red curves indicate the equivalent field strength. The curves track the antenna factor with frequency for the COMPOWER AB900 [15] bicon. Two identical AB900 antennas are used, one to search for dark photons in the shielded room, and a second to monitor the local RFI background.



Figure 2.5: Photo showing set up to measure SE of 314. Photo taken using Vivaldi antennas for data shown in Fig. 2.7. The same set up was used with bicon antennas for the 50-300 MHz data shown in Fig. 2.6. Bicon antenna shown in background of photo was not in use for this test.

## 314 Shielding Effectiveness

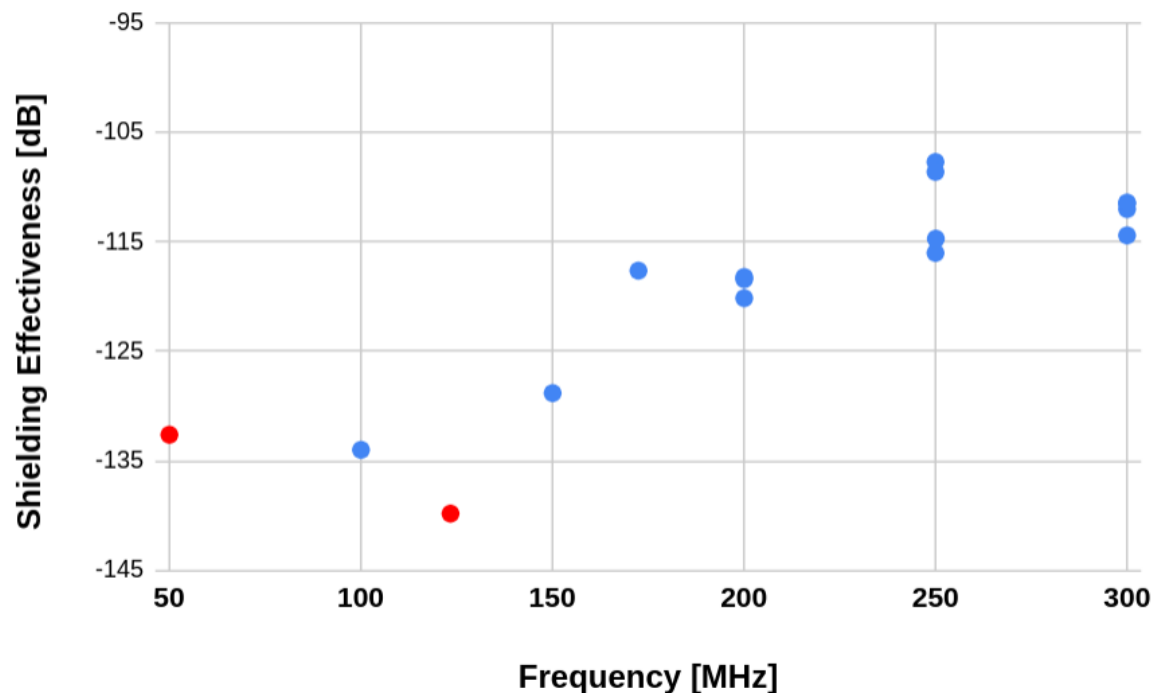


Figure 2.6: Shielding effectiveness of shielded room measured with Bicon antenna. Red points indicate measurements limited by the noise floor of the spectrum analyzer located outside and are an upper limit; true SE is lower (better). Measurement would require a stronger amplifier inside the room. At a few frequencies the antenna inside the room was moved to get a sense of the uncertainty of the measurement.

### 314 Shielding Effectiveness

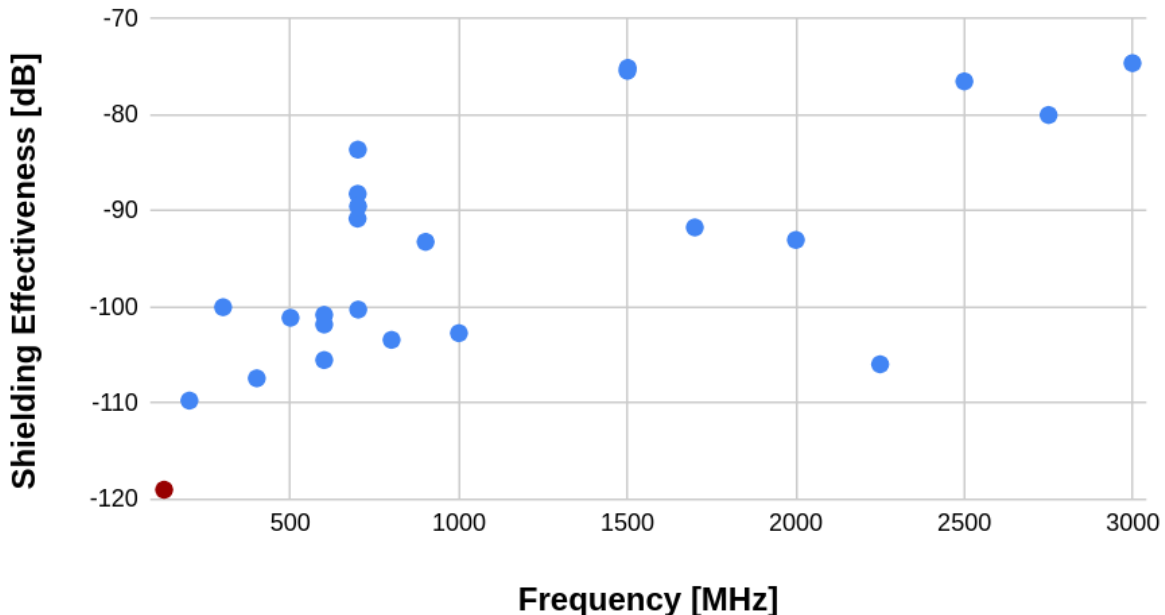


Figure 2.7: Shielding effectiveness of shielded room measured with Vivaldi antenna. Red points indicate measurements limited by the noise floor of the spectrum analyzer located outside and are an upper limit; true SE is lower (better). Measurement would require a stronger amplifier inside the room. At a few frequencies the antenna inside the room was moved to get a sense of the uncertainty of the measurement.

## 2.5.2 Antenna

The antenna plays an important roll in the experiment as the matching device between electromagnetic waves in the cavity and the receiver system. For a broadband search such as the 50-300 MHz run (a 6:1 bandwidth), a broadband antenna must be used. The chosen antenna must provide a good impedance match and high efficiency since an inefficient antenna would convert a substantial amount of the converted dark photon's power into heat in the antenna's structure. For the 50-300 MHz run, a  $\approx 131$  cm biconical antenna (bicon) was chosen. The selected model is manufactured by COMPOWER, model AB-900A [15]. In a phone call with the manufacturer as well as testing of the isolated balon, it was determined that the balun used in the antenna was 1:1. This allows for simple simulation. In COMSOL, the lumped port option allows for a balanced drive of an antenna. A match to a  $50 \Omega$  transmission line through a 1:1 balun is simply modeled as a lumped port, a very simple object in COMSOL featured in nearly all of the antenna tutorials<sup>3</sup>

---

<sup>3</sup>See for example the dipole antenna tutorial, available at <https://www.comsol.com/model/dipole-antenna-8715>

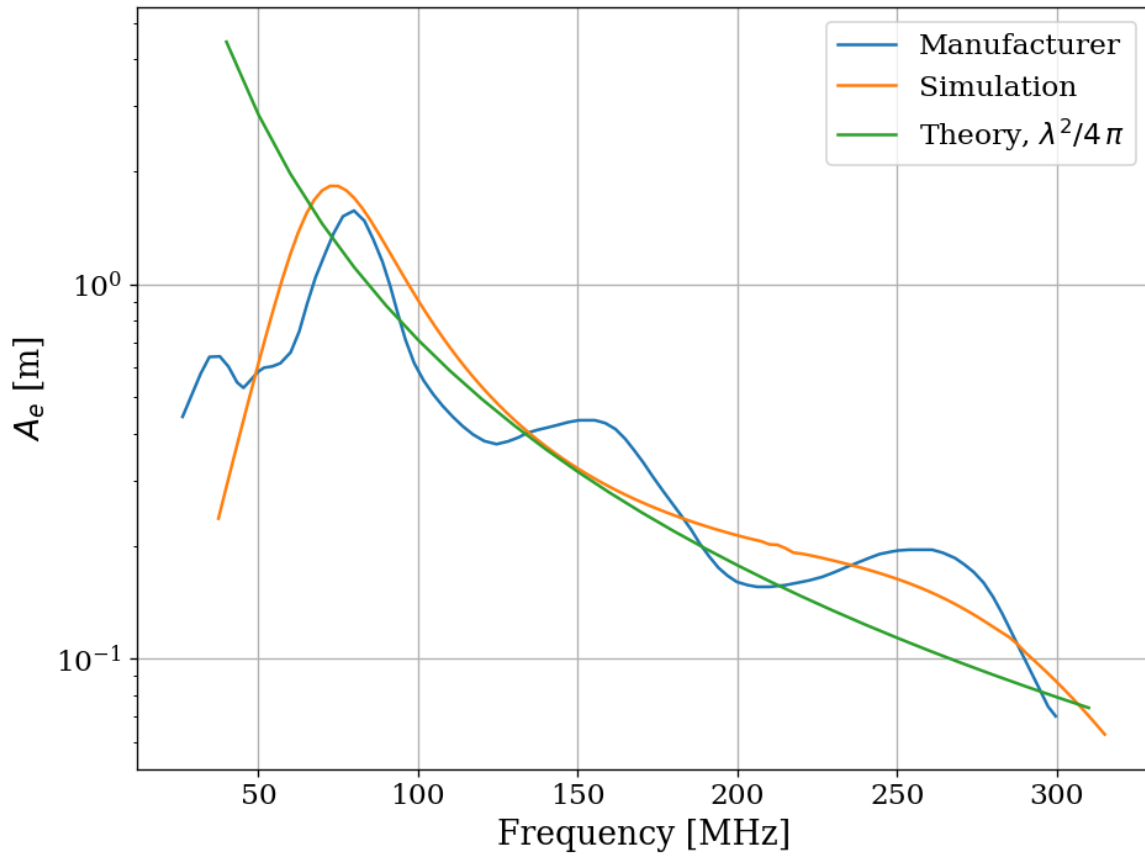


Figure 2.8: AB-900A biconical antenna effective aperture, simulated, measured and theoretical in free space. Simulation performed in COMSOL. The measurement was provided by manufacture [15] as an antenna factor and was converted using Eq. xxxx.

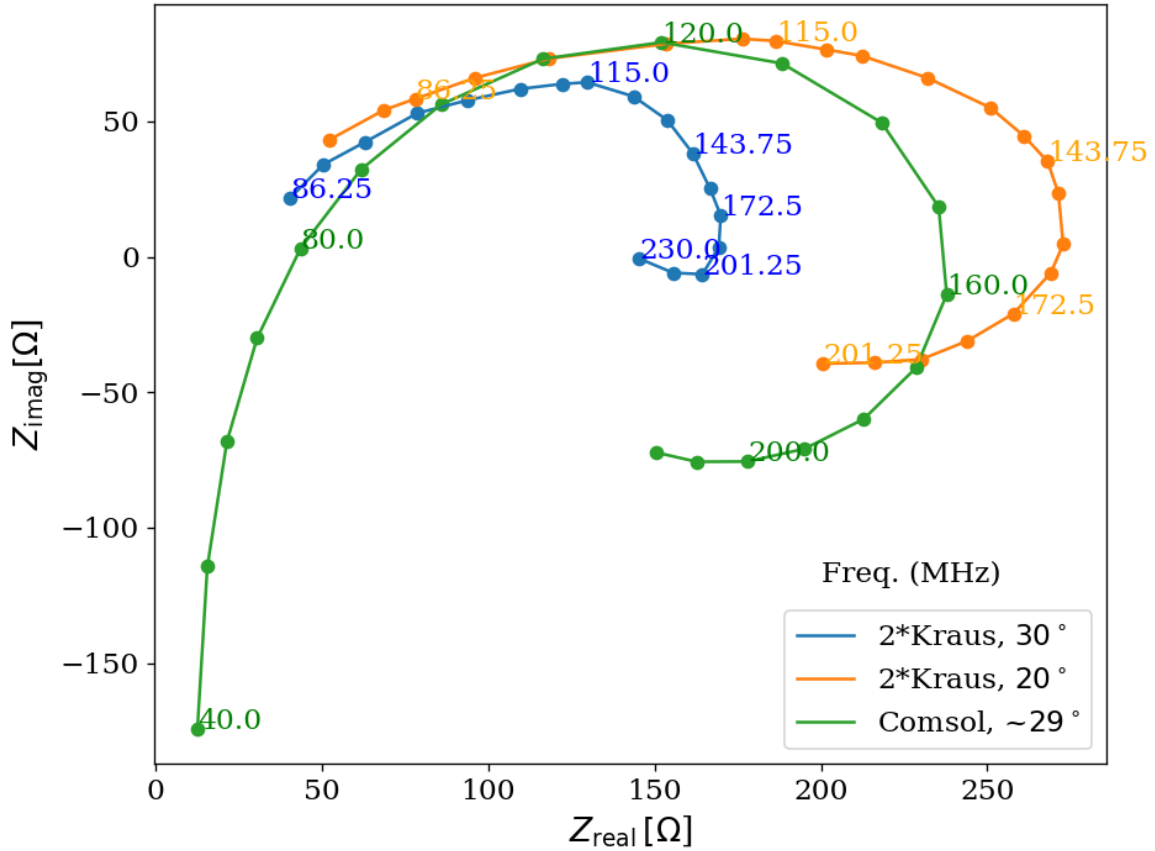
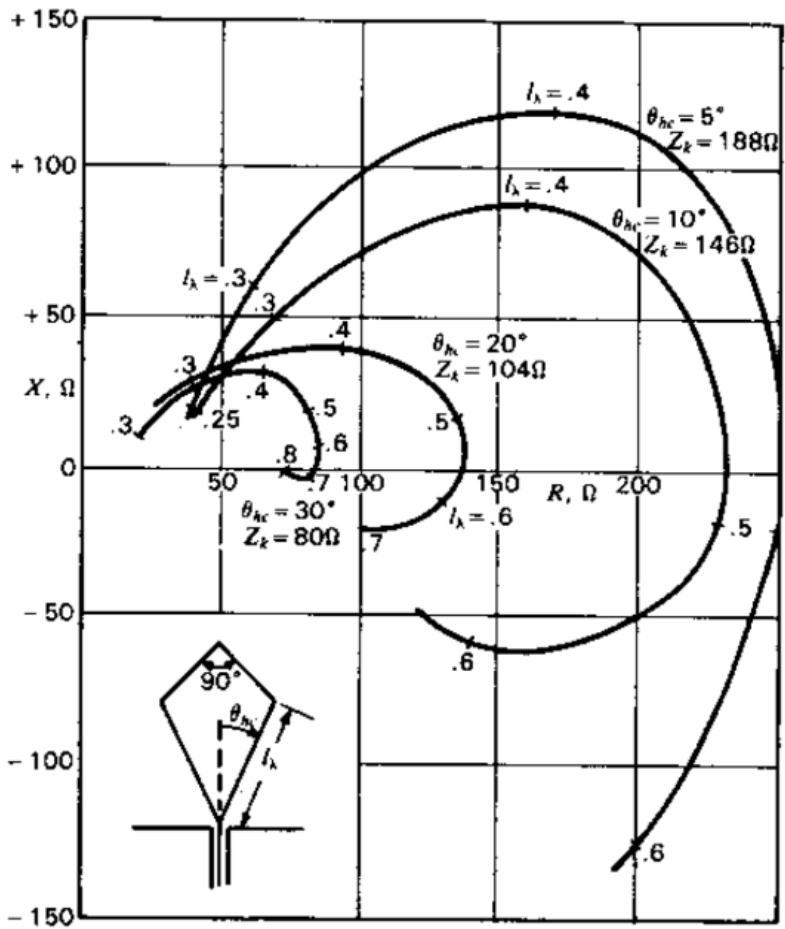


Figure 2.9: Simulated AB-900A biconical antenna free space complex input impedance shown in blue. Simulation was performed in COMSOL. Measurement from Kraus, second edition, Fig 8-13 [16], reproduced here in Fig. 2.10. Measured data is for a monoconical antenna and must be multiplied by 2 to compare to a biconical antenna. Numbers along curve indicate frequency in MHz.



**Figure 8-13** Measured input impedance of single cones with top hat as a function of cone length in wavelengths ( $l_\lambda$ ). Impedance curves are presented for cones with half-angles of 5, 10, 20 and 30°.

Figure 2.10

### 2.5.3 Terminator and switch

### 2.5.4 Low noise amplifier

### 2.5.5 Signal conditioning

### 2.5.6 Veto antenna

### 2.5.7 12 V power system

asdf

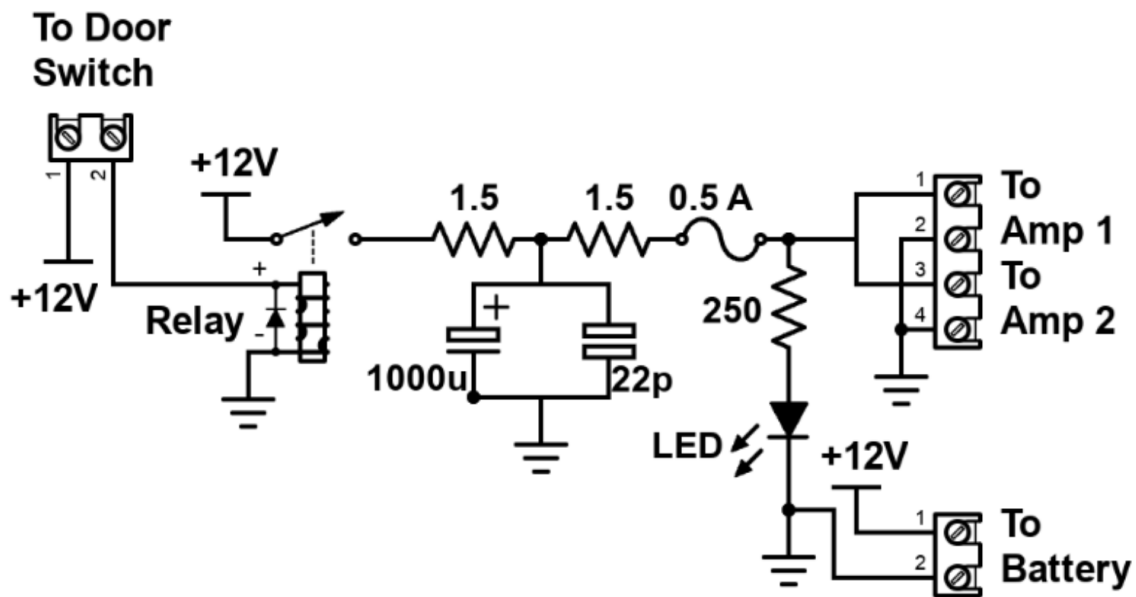


Figure 2.11: Schematic of Interlock board. No voltage regulation is provided because it is designed to work with amplifiers containing internal regulation (Pasternack PE15A1012). Not shown is a simple "slow turn on circuit" consisting of a 0.68 F capacitor and a  $8\Omega$ , 10 W resistor (time constant = 5.4 seconds) which was installed to protect the amplifier from transient voltages when the door is closed. Experience has shown the liberal use of fuses to be prudent when working with car batteries in a metal room.

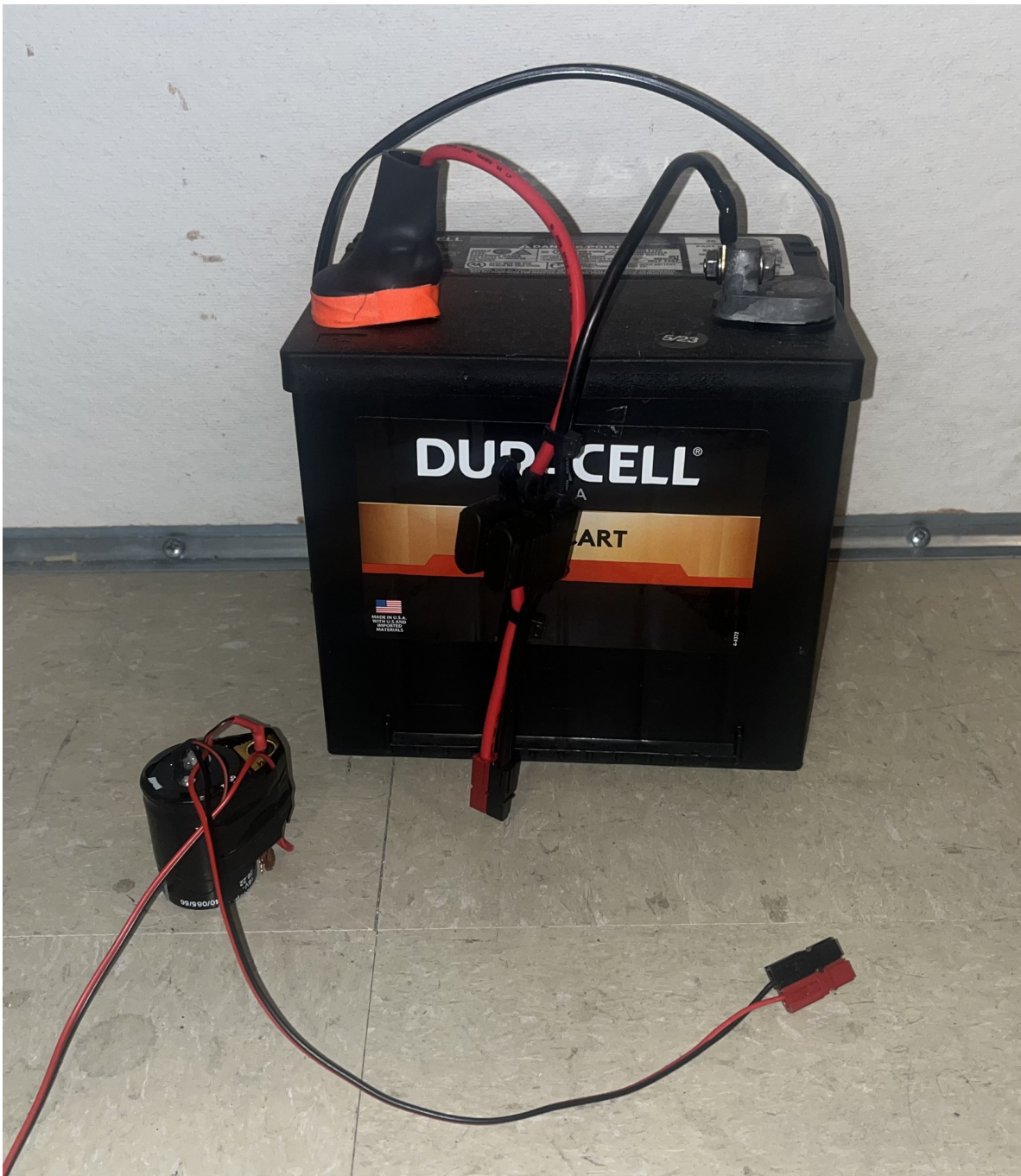


Figure 2.12: Photo of 12V lead-acid battery and slow turn on circuit. Both connect directly to the interlock board shown in Fig. 2.11. Slow turn on circuit is connected between interlock board and amplifier. Battery includes a 2A fast fuse installed in commercial Anderson power pole assembly.

### 2.5.8 GPU-Based Real-Time Spectrum Analyzer

The use of commercial Spectrum Analyzers (SAs) which feature so called RTSA (real time spectrum analyzer) mode come with several restrictions which limit the efficiency with which they are able to perform wide-band scans with narrow frequency resolution as we point out in our pilot run [**GroupPaper**]. The number of frequency bins output by an discrete Fourier transform (DFT) is equal to the number of time domain samples/2, while the bandwidth is given by sample rate/2. Furthermore, the ability to acquire data in real time requires a DFT algorithm (generally implemented as a fast Fourier transform, FFT) and computation resources which can operate on time domain data at least as fast as it is acquired. From a practical perspective this means that high frequency resolution, wide bandwidth, real time DFTs require modest memory, transfer rates and processing resources. By employing frequency mixers, restrictions on bin counts, and dead time between acquisitions, commercial SAs are able to reduce hardware demands. For this reason we have constructed our own SA based on the Teledyne ADQ32 PCIE digitizer. As a point of reference, the system used in this data run has the specifications outlined in table 2.1. While modest by modern PC standards, these specifications are generally not implemented in commercial SAs.

Bit depth	16 bits
Sample rate	800MHz
DFT input length	$2^{24}$ samples
FFT compute time	2 ms
Channel count	2

Table 2.1: Specifications for the spectrum analyzer used for run 1A.

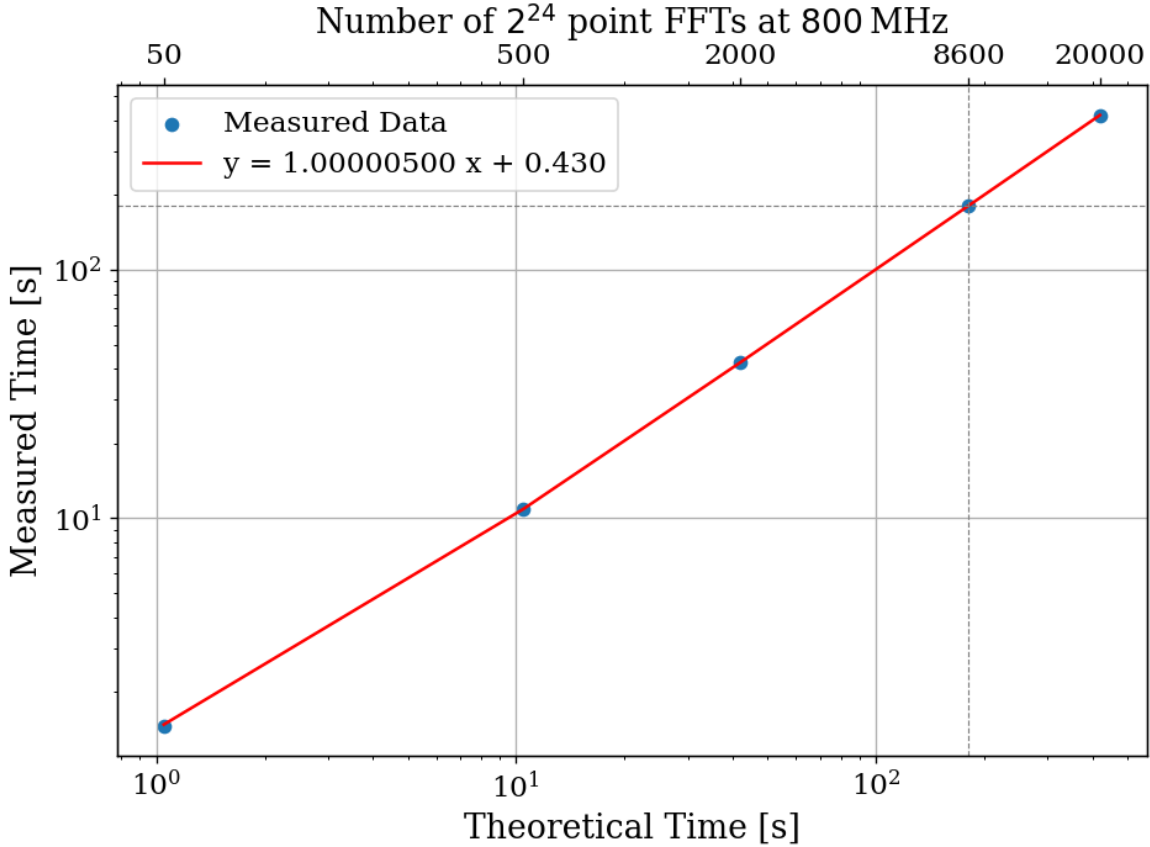


Figure 2.13: Acquisition efficiency for GPU-based Real-time spectrum analyze computed from measured vs theoretical times. The constant offset of 0.43 seconds corresponds to a small set up period when starting an acquisition containing, in the case of run 1A, 8600 FFTs. In the limit of an infinite length acquisition, the system's efficiency can be read off from the slope and is 99.9995%. The more realistic efficiency is a function of number of FFTs per acquisition and for run 1A =  $180.3551 \text{ [s]} / 180.7782 \text{ [s]} = 99.765\%$ .

### 2.5.9 Spectrum Analyzer Details

After passing through and amplifier and filter chain outlined in section ??, both the main and external antenna signals are digitized by the ADQ32's two ADCs. We utilize a GPU direct write in order to minimize CPU-GPU copies which in our experience tend to be significantly slower than the FFT itself. This GPU direct write is implemented by the digitizer's C++

API. First, several buffers are allocated in GPU memory.

Once written to a pre-allocated, time-domain buffer in the GPU’s memory, an FFT is performed using Pytorch which we found to be the fastest across all the GPUs we tested (all Nvidia). [17]



# Chapter 3

## System Characterization and Data Acquisition

“When you can measure what you are speaking about and express it in numbers you know something about it; but when you cannot measure it, when you cannot express it in numbers your knowledge is of meagre and unsatisfactory kind; it may be the beginning of knowledge but you have scarcely progressed in your thoughts to the stage of science whatever the matter may be.”

- Schematic of experiment
- Detailed schematic of amp chain
- Reason for switching. Cite dickie thermal equilibrium of resistor and antenna in cavity [18]. See 5.9.23 Messing around with different loads in lab book for experiment.

FROM PAPER 1A DRAFT: The dark E-field radio experiment consists of a biconical E-field antenna inside of a cavity. The cavity is implemented as a room temperature commercial shielded room (maufactured by ETS Lindgrin) which serves both to isolate the experiment from external radio frequency interference (RFI) and to provide resonant enhancement of any (coherent?) dark photons after they have converted to standard photons. A low noise amplifier (LNA), secondary amplifier, attenuation and a band pass filter provide analog signal conditioning before the signal is digitized by a GHz ADC (Teledyne ADQ-32), see figure 2.3. From the digitizer, records of length  $2^{24}$  are written to a GPU where a fast Fourier transform (FFT) is performed. Approximately 8000 FFTs are performed and added to a running total on the GPU (representing about 3 minutes of real time data) before dividing by the number of FFTs and copying this averaged spectrum to RAM where it can be saved for future processing, including further averaging. This pre-averaging reduces the  $\approx 3$  GB/s/channel data stream from the ADC to the GPU down to  $\approx 0.3$  MB/s/channel which allows for real time copies from the GPU to RAM but comes at the cost of temporal resolution of transient candidates. This is summarized in Fig. 3.1.

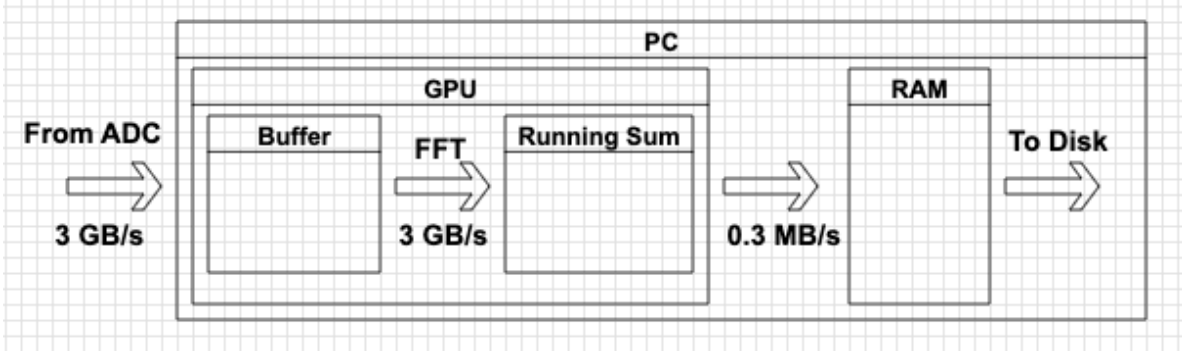


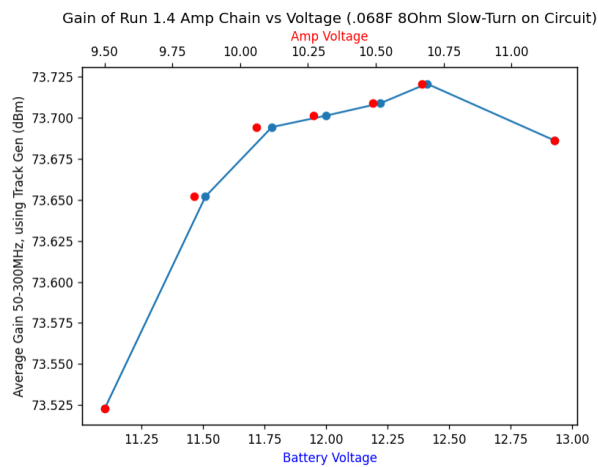
Figure 3.1: Data stream of real time DAQ. This set up is duplicated for channels A and B

## 3.1 Control and Quantifying of Uncertainties

### 3.1.1 Direct Measurement of Amp Chain Parameters

- Gain
- Noise schematic

Figure 3.2: Gain vs. voltage of front end amplifier



# Chapter 4

## Data Analysis and Calibration

We will build up this search in two successive steps. First a basic analysis on the averaged spectrum (roughly equivalent a *processed spectrum* in [haystac’2017]) which sets a relatively simple, though conservative limit. The second step accounts for the variation of Q with frequency. This comes into play because a dark photon line with  $Q = 1\text{e}6$  would span a single 50 Hz bin at 50 MHz but would span 6 bins at 300MHz. This is accomplished with a signal-matched filter in the frequency domain to improve SNR by compressing the signal’s power into as few bins as possible. We observe a small improvement at 50MHz (where the signal is expected to span only a bin or two) and a factor of XXXX improvement at 300MHz, and a linear(JL: check this claim) improvement-factor between these two extremes.

Following an exploration of the details of the analysis pipeline, we take a step back and place the analysis in a black box and perform a Monte Carlo validation of our sensitivity by injecting signals onto a generated background. Our background is white noise riding on a slowly varying undulations and is therefore simple to generate. We employ a simple Monte Carlo method to find the XXXX% confidence limit on power which we would be able to detect. In the absence of a signal, this limit on power can be converted into a limit on epsilon.

# Chapter 5

## Beyond 300 MHz

To infinity and beyond!

---

Buzz Lightyear

# Bibliography

- [1] Fritz Zwicky. “The Redshift of Extragalactic Nebulae”. In: (1933).
- [2] Vera C. Rubin and Jr. Ford W. Kent. “Rotation of the Andromeda Nebula from a Spectroscopic Survey of Emission Regions”. In: (1970).
- [3] Marco Battaglieri *et al.* *US Cosmic Visions: New Ideas in Dark Matter 2017: Community Report*. 2017. DOI: 10.48550/ARXIV.1707.04591. URL: <https://arxiv.org/abs/1707.04591>.
- [4] V. Radeka. “Signal, Noise and Resolution in Position-Sensitive Detectors”. In: *IEEE Transactions on Nuclear Science* 21.1 (1974), pp. 51–64. DOI: 10.1109/TNS.1974.4327444.
- [5] David Hill. “Plane Wave Integral Representation for Fields in Reverberation Chambers”. en. In: 40 (1998-08-01 00:08:00 1998).
- [6] W. L. Stutzman and G. A. Thiele. *Antenna Theory and Design*. John Wiley Sons, 1998.
- [7] J.D. Kraus. *Antennas*. McGraw-Hill, 1950. ISBN: 07-035410-3.

- [8] Raphael Cervantes et al. *Deepest Sensitivity to Wavelike Dark Photon Dark Matter with SRF Cavities*. 2022. arXiv: 2208.03183 [hep-ex].
- [9] Pasternack Enterprises. *PE15A1012: 1 Watt Amplifier Operating From 0.01 GHz to 6 GHz*. Accessed: 2024-05-17. 2024. URL: <https://www.pasternack.com/images/ProductPDF/PE15A1012.pdf>.
- [10] *Series 83 RF Shielded Enclosure*. Lindgren R.F. Enclosures, Inc. 2021. URL: <https://www.ets-lindgren.com/datasheet/shielding/rf-shielding-and-accessories/11003/1100307>.
- [11] David A. Hill. *Electromagnetic Theory of Reverberation Chambers*. Technical Note 1506. Gaithersburg, MD: National Institute of Standards and Technology, 1998. URL: [https://tsapps.nist.gov/publication/get\\_pdf.cfm?pub\\_id=24427](https://tsapps.nist.gov/publication/get_pdf.cfm?pub_id=24427).
- [12] D.A. Hill. “A reflection coefficient derivation for the Q of a reverberation chamber”. In: *IEEE Transactions on Electromagnetic Compatibility* 38.4 (1996), pp. 591–592. DOI: 10.1109/15.544314.
- [13] Lawrence Krauss et al. “Calculations for cosmic axion detection”. In: *Physical Review Letters* 55.17 (1985), pp. 1797–1800. DOI: 10.1103/PhysRevLett.55.1797. URL: <https://doi.org/10.1103/PhysRevLett.55.1797>.
- [14] “IEEE Standard Method for Measuring the Effectiveness of Electromagnetic Shielding Enclosures”. In: *IEEE Std 299-1997* (1998), pp. 1–48. DOI: 10.1109/IEEESTD.1998.88115.

- [15] *Biconical Antenna AB-900A*. Rev. D05.19. Com-Power Corporation. May 2019. URL: <https://documentation.com-power.com/pdf/AB-900A-1.pdf>.
- [16] John D. Kraus. *Antennas*. 2nd. New York: McGraw-Hill, 1988, p. 892. ISBN: 9780070354227.
- [17] CuPy Developers. *CuPy: NumPy-compatible array library accelerating machine learning with CUDA*. [https://docs.cupy.dev/en/stable/user\\_guide/interoperability.html](https://docs.cupy.dev/en/stable/user_guide/interoperability.html). Accessed on: May 11, 2023. 2021.
- [18] Robert H Dicke. “The measurement of thermal radiation at microwave frequencies”. In: *Review of Scientific Instruments* 17.7 (1946), pp. 268–275.